The Chemistry of Nucleation: *In situ* Pair Distribution Function analysis of secondary building units during UiO-66 MOF formation

Hui Xu,[a,b] ‡ Sanna Sommer, [a]‡ Nils Lau Nyborg Broge,[a] Junkuo Gao,[c] and Bo. B. Iversen*[a]

Abstract: The concept of Secondary Building Units (SBUs) is central to all science on metal-organic frameworks (MOFs), and they are widely used to design new MOF materials. However, the presence of SBUs during MOF formation remains controversial, and the formation mechanism of MOFs remains unclear due to limited information about the evolution of prenucleation cluster structures. Here *in situ* Pair Distribution Function (PDF) analysis was used to probe UiO-66 formation under solvothermal conditions. The expected SBU - a hexanuclear zirconium cluster - is present in the metal salt precursor solution. Addition of organic ligands results in a disordered structure with correlations up to 23 Å resembling crystalline UiO-66. Heating leads to fast cluster aggregation, and further growth and ordering results in the crystalline product. Thus, SBUs are present already at room temperature and act as building blocks for MOF formation. The proposed formation steps provide insight for further development of MOF synthesis.

Introduction

Metal Organic Frameworks (MOFs) constitute a fascinating class of crystalline porous materials with applications in many different areas such as gas storage/separation, luminescent sensing, drug delivery and photocatalysis.[1] The idea of "designing" LEGO™ like MOF structures is generally considered to involve choosing a metal polyhedron unit, or so-called secondary building unit (SBU), with known coordination preferences, and then link these with organic ligands to form predictable three-dimensional frame works.[2] This is currently possible to a limited extent, despite the relatively poor evidence for the actual atomic-scale mechanisms of MOF formation in solvothermal synthesis. This gap in knowledge hampers both the preparation of new MOFs as well as the ability to precisely control their crystal growth and morphology.

Research on the mechanism of crystal nucleation and growth is an important area in physics, chemistry, materials science and environmental research.[3] As an example crystal nucleation and growth plays an important role for controlling the morphology and facets in metal nanocatalysts,[4] and it is also crucial in our daily life e.g. for the formation of atmospheric particles.[5] Clearly, a proper understanding of prenucleation processes as well as the mechanisms controlling nanocrystal properties is highly desired. The prevailing nucleation and growth models range from classical LaMer and Johnson-Mehl-Avarami models to newer pre-nucleation cluster and oriented attachment models.[6] These models have been used to describe nucleation and growth in many different cases based on a simplified notion of "particles" or "monomers", but with limited consideration given to the atomic scale nature of a system. In general, there is limited understanding of the underlying "chemistry" of nucleation and growth processes.

The study of MOF formation has been based on different techniques with different strengths, which when used in conjunction overcome their individual shortcomings.[7] *In situ* energy-dispersive powder X-ray diffraction (PXRD) is an appropriate technique to investigate the formation and evolution of crystalline MOF phases.[8] Interesting metastable intermediates and interconversion of MOFs were observed through *in situ* PXRD measurements, which provided a comprehensive picture of MOF crystallization.[7, 9] Small Angle X-ray Scattering (SAXS) was used to probe the precursor clusters and the nanocrystal formation mechanisms in order to overcome the limitations of PXRD for analyzing the processes occurring before crystallization. However SAXS is not able to reveal atomistic structural details of the nucleation and growth processes.[10] Therefore, MOF formation remains a black box without atomic scale insight.

SBUs are the conceptual basic building units and their connectivity greatly influences final MOF topology.[11] A few pioneering studies based on a two step crystal engineering strategy relied upon first preparing the SBUs and then constructing tunable MOF structures,[12] but due to inherent limitations of the techniques used, the cluster structure of MOF precursor species in homogenous solution is still unknown. Furthermore, the actual formation of MOF SBUs in solution prior to, or during, crystallization continues to be a source of contention.[7] The pioneering work by Ferey utilized *ex situ* EXAFS and NMR to verify the SBU hypothesis, and their findings indicated that SBUs form prior to MOF crystallization, and can be retained during MOF synthesis.[13] On the other hand, the AFM work by Shoaee on HKUST-1 does not support this conclusion, and rather suggests that monomers and isolated ligands are the basic growth units.[14] The techniques employed by both these studies are constrained by an inability to provide direct structural evidence for the presence of SBUs prior to and during MOF crystallization, and therefore cannot definitively answer if SBUs contribute to MOF formation or not.

In situ X-ray total scattering is a powerful tool for studying materials formation mechanisms under solvothermal synthesis conditions, as it allows extraction of structural information from amorphous materials (including gases and liquids), short-range

[a] Dr. H. Xu, S. Sommer, N. L. N. Broge, Prof. Dr. B. B. Iversen
Center for Materials Crystallography
Department of Chemistry and iNANO, Aarhus University
Langelandsgade 140, 8000 Aarhus (Denmark)
E-mail: bo@chem.au.dk
[b] Dr. H. Xu
College of Materials Science and Engineering, China Jiliang University, Hangzhou 310018, P. R. China
[c] Prof. Dr. J. Gao
College of Materials and Textiles, Zhejiang Sci-Tech University, Hangzhou 310018, P. R. China
‡ Both authors have equal contribution to this paper.

Supporting information for this article is given via a link at the end of the document.

order nano-particles, and long-range order crystalline particles. Pair distribution function (PDF) analysis, obtained by Fourier transformation of the total scattering structure factor S(Q), provide a histogram of all interatomic distances in the sample ("fingerprint").[15] *In situ* total scattering has previously been used to reveal a rich chemistry in the nucleation and growth of inorganic materials such as CeO_2, SnO_2, ZrO_2, Fe_2O_3, WO_3 and $ZnWO_4$.[16]

In the field of MOFs, work by Chapman *et al.* utilized PDF analysis to probe local structural transitions of M_6O_8 nodes during heating UiO-66 and NU-1000 in dry powder form.[17] Recently, the pioneering work by Billinge *et al.* combined multiple techniques such as *in situ PDF,* mass spectrometry and DFT calculations to reveal the early stage structural development of prototypical zeolitic imidazolate framework in solution.[18] These results showed the promise of PDF analysis of SBU structures, and inspired the present *in situ* study of the solvothermal formation of UiO-66. Since the SBUs in MOFs consist of metal-oxide clusters, we chose a relatively heavy metal MOF system to generate strong X-ray scattering. This facilitates the possibility to catch a glimpse of the fundamental chemical transformations taking place before and during the initial nucleation stage as well as the evolution of the cluster structure during early growth. Here, we present an *in situ* PDF study on the solvothermal synthesis of UiO-66.

Results and Discussion

Cluster formation in the UiO-66 solution before addition of the organic linker

We first study the nature of the solution of the metal source before addition of the organic linker. As shown in Figure 1a, the most prominent features of the dissolved Zr(IV) precursor ($ZrCl_4$) in DMF and HCl solution (PH=1.8) are the intense PDF peaks at 2.2, 3.5 and 5.0 Å. No correlations are observed above 8 Å (Figure 1(a)), which suggest that no clusters larger than 8 Å exist in the metal precursor solution. This led us to consider that the species in this metal salt solution may be the UiO-66 SBU $Zr_6(O)_4(OH)_4$ structure, which is a Zr_6-octahedron bridged by μ3-O and μ3-OH groups, and with main Zr···O and Zr···Zr distances of 2.2, 3.5 and 5.0 Å, respectively.[19] The PDF is unable to differentiate whether there is hydrogen present because of the weak scattering from hydrogen. Thus, the UiO-66 SBU structure was isolated from the crystal structure (ICSD-4512072),[19] yielding a hexanuclear Zr cluster ($Zr_6(O)_8(O)_{24}$), which has eight faces of a regular octahedron bridged by eight μ3-oxygen atoms and the cluster is terminated by 24 oxygen atoms from solvent H_2O or DMF to ensure a saturated coordination, as shown in Figure 1b. The main atom distances in this SBU includes the Zr-O bond at approximately 2.2 Å, the Zr···Zr distances across the edges of the octahedron at approximately 3.5 Å, and the diagonal Zr···Zr distances inside the SBU at approximately 5.0 Å. The Zr···Zr distances at 3.5 Å and 5.0 Å are associated with 12 and 3 equivalent distances, respectively, which determines the PDF peak area. The hexanuclear SBU was modelled against the PDF data using the program DiffyCMI,[20] and acceptable fits were obtained both for $ZrCl_4$ in DMF-HCl solution (Figure 1(a)) as well as for $ZrCl_4$ in DMF-H_2O solution (see supporting information section 7 for details and fitting results). Only simple models were applied in order to confirm the presence of the clusters, and no modelling of solvent effects, correlated movements etc. was undertaken. Such effects contribute to a broadening of the peaks and lead to residual intensity between the model and the observed PDF. The PDF show a strong similarity to the PDF features below 7 Å for amorphous and crystalline UiO-66,[17, 21] supporting that the observed cluster structure closely resemble the SBU for the UiO-66.

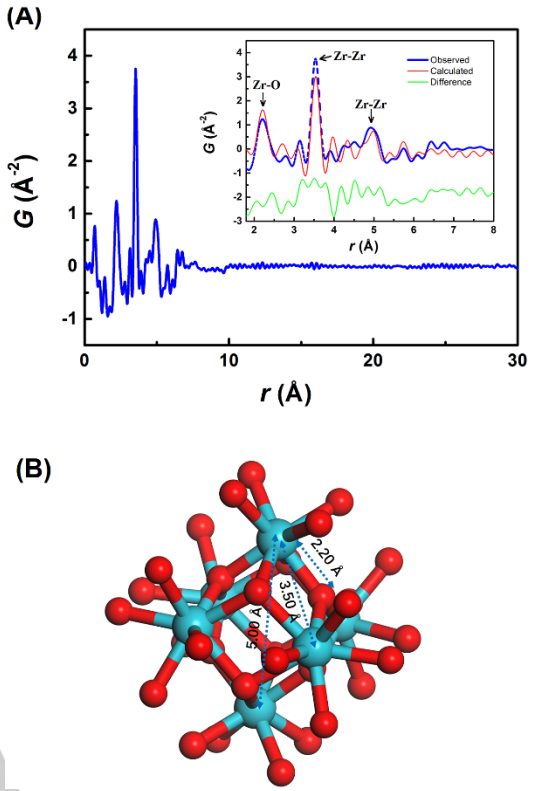

Figure 1. A) PDF for the solution of $ZrCl_4$ in DMF and HCl. Inset shows enlarged PDF for the solution of $ZrCl_4$ in DMF-HCl fitted with hexanuclear Zr cluster SBU model. B) Hexanuclear Zr cluster obtained from fitting the data in A (red: oxygen atom; blue: Zr atom). The PDF data were modelled using DiffPyCMI.[20]

Previous research has systematically studied the structure of Zr(IV) multinuclear species in various solutions from different precursor salts by EXAFS, mass-spectrometry and computational studies,[22] which indicated that zirconium shows a strong tendency toward hydrolysis and polymerization. There is a common agreement that the tetramer complex $Zr_4(OH)_8(H_2O)_{16}$ with extraordinary stability is the dominant hydrolysis species in zirconium aqueous solution;[22a-c, 23] while the extended oligomer chains $Zr_8O_{28}(NO_3)_8$ is the dominant species in Zr oxynitrate in methanol or Zr acetate aqueous solution.[22d, 24] In the current study, it is clear that neither the tetramer species nor the extended oligomer chains explain the higher peak area of 3.5 Å than 2.2 Å, which shows disagreement with the experimental PDF of the dissolved Zr(IV) precursor in DMF and HCl solution (Figure S9-S10). On the contrary, the UiO-66 SBU (hexamer) is a more suitable model and provides improved fits compared to the $Zr_4(OH)_8(H_2O)_{16}$ and $Zr_8O_{28}(NO_3)_8$ cluster (Figure S8). This indicates the predominant presence of UiO-66 SBU structures in $ZrCl_4$ precursor solution without addition of organic ligand. This

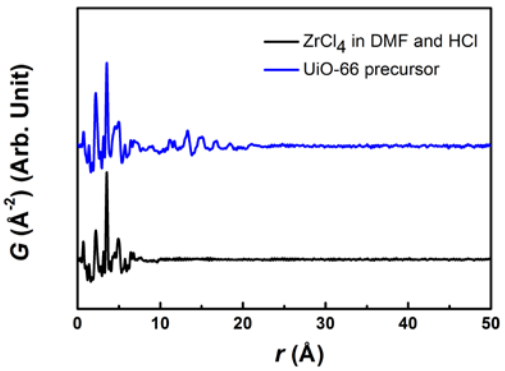

Figure 2. PDF comparison of the UiO-66 precursor solution (blue) and $ZrCl_4$ in DMF-HCl (black).

hexanuclear zirconium cluster has previously been observed as dominant structure in Zr(IV) aqueous solution with addition of acetic acid (pH = 1.5) by EXAFS.[22c] However, the present PDF analysis is the first evidence of this SBU existing at room temperature in the metal source precursor solution usually used for UiO-66 synthesis.

Cluster formation in the UiO-66 precursor solution prior to heating

Next the complete UiO-66 precursor solution was studied before heating by adding the organic ligand to the solution of $ZrCl_4$ in DMF-HCl (pH = 1.8). This solution was stirred until transparent to make the UiO-66 precursor solution, and the resulting PDF is shown in Figure 2. The observed PDF is dominated by atom−atom correlations involving the strongly scattering Zr atoms. Compared with the PDF of the $ZrCl_4$ solution (Figure 2), the UiO-66 precursor shows structural correlations to larger distance. In the UiO-66 precursor solution the correlations extend to beyond 20 Å, indicating that larger clusters form spontaneously upon addition of the organic ligand. According to the modelled sp-diameter in the xPDF-suite software, the predominant cluster size is 23 Å. At this stage the clusters are still solution species rather than precipitated nanoparticles, as shown by the transparent UiO-66 precursor solution (Figure S50).

The PDF can be divided into two parts with distances below 8 Å, and distances above 8 Å. In the d < 8 Å range, the main peaks remain at 2.2, 3.5 and 5.0 Å, corresponding to the Zr-O and Zr···Zr distances inside one SBU. This indicates that the MOF SBU structure is still the basic structure in the larger cluster of the complete precursor solution. In the d > 8 Å range, new main peaks appear at 11.2, 13.3, 15.1, 16.8 and 18.5 Å. They correspond to Zr···Zr atom distances between two different SBUs connected by the organic linker, indicating that the cluster is an assembly of several SBUs, and the cluster structure resembles UiO-66 crystal structure.[19]

Different cluster models were established based on different fractions of the UiO-66 crystal structure,[19] namely 3SBU, 4SBU, 5SBU and 6SBU, etc., according to the number of SBUs each cluster contained (Figure S17-27). Firstly, the different clusters were modelled against the whole PDF modelling (r ranging from 1.8-30 Å). The higher degree of disorder at large r values complicates a complete refinement of the datasets (Figure 3b,

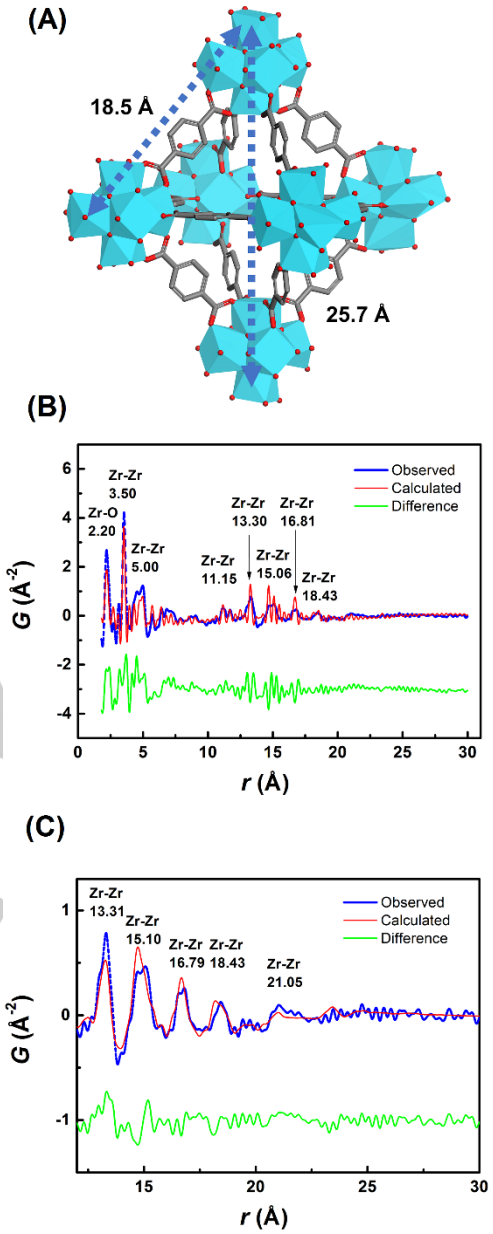

Figure 3. A) Octahedral cluster (6 SBU) present in the UiO-66 precursor solution. (red: oxygen atom; blue polyhedron: Zr atom) B) Full range PDF for the UiO-66 precursor solution fitted with octahedral 6 SBU cluster and fixed atomic displacement parameters (ADPs). C) High r range PDF for the UiO-66 precursor solution fitted with octahedral 6 SBU cluster with refined ADPs. The high-r fit is significantly improved with refined ADPs, most likely because these account for dynamic effects such as rigid body movement of linked SBUs.

Figure S28-38 and Table S6). A high r region (12-30 Å) was refined separately where the disorder was allowed to be absorbed into the atomic displacement factors (ADP). This approach gave models with a lower residual than the full range modelling (Figure 3c, Figure S39-46 and table S8). According to the high r range modelling, 2-5 SBUs models provide high R_w and unsatisfactory

fits (Figure S39-42 and Table S8); while 6-9 SBUs provide reasonable fits. However they are difficult to distinguish due to experimental and modelling limitations (Figure S43-46 and Table S8). The similar R_w values between the 6-9 SBUs models also indicate that a cluster size distribution is present in the precursor solution. Based on visual inspection of the dampening of the peaks, the 6-7 SBUs are the predominant cluster sizes. Thus the high r range refinements suggest that the majority of the clusters present are 6-7SBUs (Figure S43-44). The large ADP values obtained in the refinements confirm that a substantial degree of disorder is present in the clusters.

Nevertheless residual intensity is still present between the model and the experimental PDF. This can largely be explained by two factors. Firstly, the distribution of cluster sizes and shape will provide changes in the relative ratio between the calculated PDF peaks, which may cause residual intensity. Secondly, the peaks in the observed PDF are considerably broader than the model peaks (Figure S49), which also lead to residual intensity. The broader peaks of the observed PDF compared to the model also suggests substantial degree of disorder in the cluster compared with the final UiO-66 crystal structure obtained from data on a reference powder sample. [19] It is interesting to compare the observed PDF with the pioneering work by Bennett *et al*. and Chapman *et al*. on PDF for both amorphous and crystalline UiO-66.[17, 21] The PDF features below 7 Å is very similar with both amorphous and crystalline UiO-66,[17, 21] supporting that the $Zr_6(O)_4(OH)_4$ SBU structure keep intact, and a limited structural distortion is observed; while the PDF features above 7 Å show differences with that of both amorphous and crystalline UiO-66. These peaks represent the structural features obtained by the linkage of SBUs. For the PDF features above 7 Å, the observed PDF exhibits longer range order than the amorphous UiO-66 [21] and the peak signal damping is significantly slower supporting that in the observed PDF the SBUs are linked by the ligands, in contrast to the partial isolated SBUs in the amorphous UiO-66. The observed PDF have broader peaks with lower intensity than the crystalline UiO-66, [21] equally, the peak signal damping is much faster supporting that there is a substantial degree of disorder in the cluster at this stage compared with the well-crystalized UiO-66. In agreement with previous studies on defect MOFs,[10b, 25] we speculate that the clusters, while resembling the UiO-66, still exhibit significant disorder features such as missing ligands and/or are in wrong coordination mode compared with the perfect UiO-66 crystal structure.[25b] Additionally, rigid-body motion of the cluster SBUs in solution will also broaden the peaks in the PDF.

Previously several studies have used SAXS, EXAFS, ESI-MS or NMR to demonstrate the formation of multinuclear clusters prior to MOF crystallization.[10b, c, 13a, 18, 26] For example, *in situ* SAXS studies of ZIF-8 have identified the spontaneous formation of clusters with approximately sizes of 20 Å when mixing the precursor component solution.[10c] However, SAXS cannot provide atomic level structural information, and the study only proposed the initial clusters as monodisperse homogeneous spheres while the internal atomic structure of the cluster remained unknown. Recently, a pioneering *in situ* PDF study also revealed a high concentration of $Zn(2\text{-MeIm})_4$ cluster initially formed and remained stable over long times before crystallization during ZIF formation.[18] Thus, this present study provides a direct structural evidence of the atomic structure of MOF prenucleation clusters.

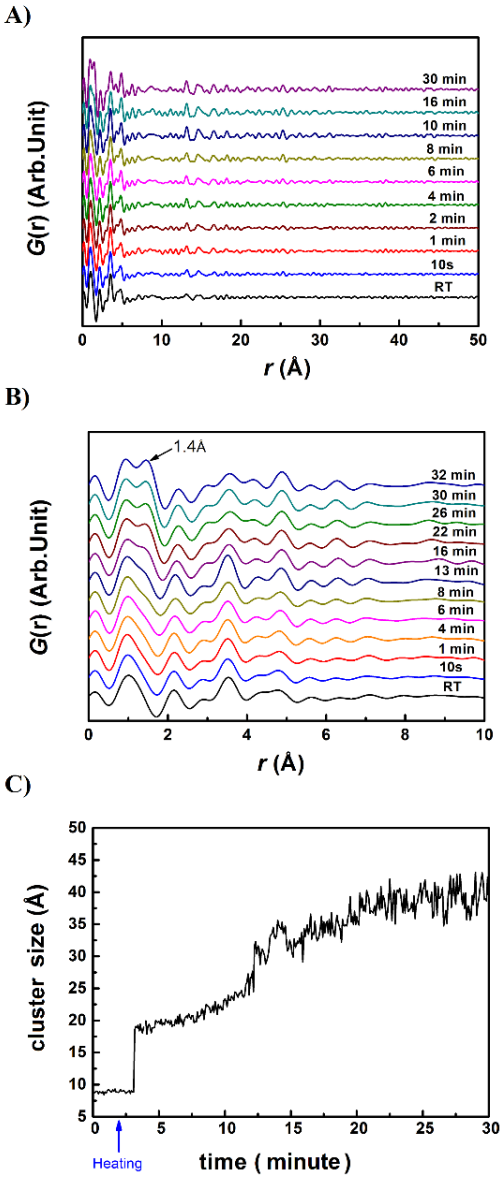

Figure 4. A) Selected PDFs illustrating the reaction progress at 150°C. B) Magnified PDFs shows the evolution of PDF at 1.4 Å with heating time at 150°C. C) The evolution of the cluster size with time.

Crystal growth and ordering upon heating

Figure 4a shows the evolution of the PDF with respect to time when heating at 150°C. The structure in solution maintains the same short-range coordination distances before and after the heating is initiated. It is worthy to note that in the short range PDF, the main atom distances of Zr-O, Zr-Zr and Zr-Zr remained at 2.2, 3.5 and 5.0 Å, respectively, and no change of main atom distances were found, indicating that there is limited distortion of SBU structure during crystallization.[17] In the long range PDF, peaks arise and grow in the regions around r = 15.0 Å and r = 25.0 Å, corresponding to inter-SBU distances in the UiO-66

crystal structure, which indicates the assembly of clusters in the precursor solution. The refined maximum correlation length increases quickly after heating is applied revealing that the cluster growth is rapid (Figure 4c). With increasing heating time, the growth rate of the cluster slows down, and the PDF peaks become more well-defined.

After 4 minutes, a very small peak (firstly as a shoulder) at 1.4 Å begins to appear and gradually becomes more well defined and increase in intensity, as shown in magnification in Figure 4b (see also Figure S51). This distance is specific for the C-N and aromatic C-C bond in the ligand. This possibly can be ascribed to ligands migrating from the solvent and into the UiO-66 structure, and due to the higher density in the crystal compared to the solvent, the 1.4 Å peak increases in intensity. The *in situ* reaction cell is not uniformly heated, meaning that the non-heated volume will act as a precursor reservoir from which the ligands might diffuse. At the same time the as-formed particles transform from their initial disordered state, which was also indicated by the initial broadening of the peaks, to a cluster that represent the UiO-66 structure more correctly with more well-defined PDF peaks. After 4 minutes, the entire PDF pattern gradually resembles the pattern from the UiO-66 crystal structure (Figure 4a). The high-r features continue to increase in intensity throughout the experiment, and this shows how full crystallization and ordering of the structure requires extended time at elevated temperature.

Due to the limitation of instrumental conditions, the noise in the *in situ* RT data at long correlation distances (>10 Å) is too high to get a precise estimate of the particle size. However, even if the absolute value of the particle size obtained from the PDF fitting should be interpreted with caution, then the trend in the crystal growth should be correct. Figure 4c reveals the evolution of the relative growth of the cluster size over time, and a gradual increase in cluster size is observed following a sudden jump at approximately 70 s after initiation of heating has commenced. This can be ascribed to the fast aggregation of the multinuclear clusters in UiO-66 precursor solutions. It is worth to mention that the aggregation process has also been observed to be exist as an independent process before fully crystallization, based on the SAXS, WAXS and DFT analysis by the groups of Goesten and Gascon.[10b] A slight increase in the cluster size is observed beyond the last measurement at about 32 min. Modeling of the PDF obtained at the last measurement with the final UiO-66 crystal structure gives a satisfactory fit (Figure S52), demonstrating successful synthesis of UiO-66 nanocrystals during the *in situ* synchrotron experiment.

To further analyze the UiO-66 crystallization process we performed synthesis using the same precursor in a reactor that mimics the *in situ* conditions (Figure 5).[27] Three main features were obtained from Rietveld refinement of these PXRD patterns. Firstly, Rietveld refinements of the PXRD of the sample synthesized at 150 °C for 60 minutes agrees well with the crystallographic database[19] (Figure 5b), which also verifies the successful synthesis of UiO-66 crystalline nanoparticles. Secondly, the 3 min sample contains both the characteristic Bragg peaks for UiO-66 and some very broad peaks, which indicates the coexistence of crystalline particles and clusters that are yet to assemble into crystalline particles. And thirdly, the PXRD crystalline size of the 3 min and 60 min samples are 3.4 nm and 7.0 nm, respectively, based on Rietveld refinements. This agrees with the PDF refinement results where the cluster size first quickly increases followed by a slower growth during which the particles undergo structural ordering.

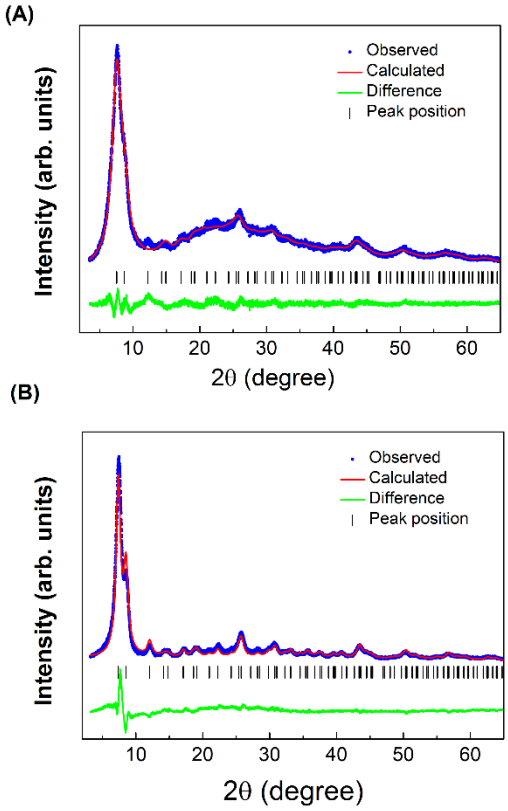

Figure 5. Rietveld refinement of PXRD data of UiO-66 synthesized using the same precursor solution using a synthesis reactor that mimics the *in situ* conditions,[27] at 150 °C for (A) 3 min. (B) 60 min.

Summary: Formation mechanism of UiO-66

Overall, the UiO-66 formation process can be described in four steps:

- Step 1, The hexanuclear SBU structure is formed in the $ZrCl_4$ metal salt precursor solution
- Step 2, Assembly of multinuclear clusters containing SBUs takes place with addition of organic ligand in UiO-66 homogenous precursor solution
- Step 3, The multi-SBU clusters quickly aggregate soon after heating is applied
- Step 4, The UiO-66 structure undergoing ordering and growth gradually become fully crystalline.

Figure 6 summarizes the species detected by the PDF and PXRD analysis from the initial precursor cluster to the formation of final UiO-66 nanocrystal.

The aggregation of large molecular clusters with subsequent internal ordering is highly complex, and not described by classical nucleation theory, where thermodynamic energy is understood to lead to a critical nucleus size in a supersaturated solution. The observed nucleation of UiO-66 exhibits similarities with the pre-nucleation clusters (PNC) model, where “the PNCs are amorphous or nano-crystalline assemblies of atoms in a structurally stable, yet soluble entity”.[28] The precursor cluster in

UiO-66 is very large at approximately 2.3 nm, which is almost one unit cell of the final crystal structure.

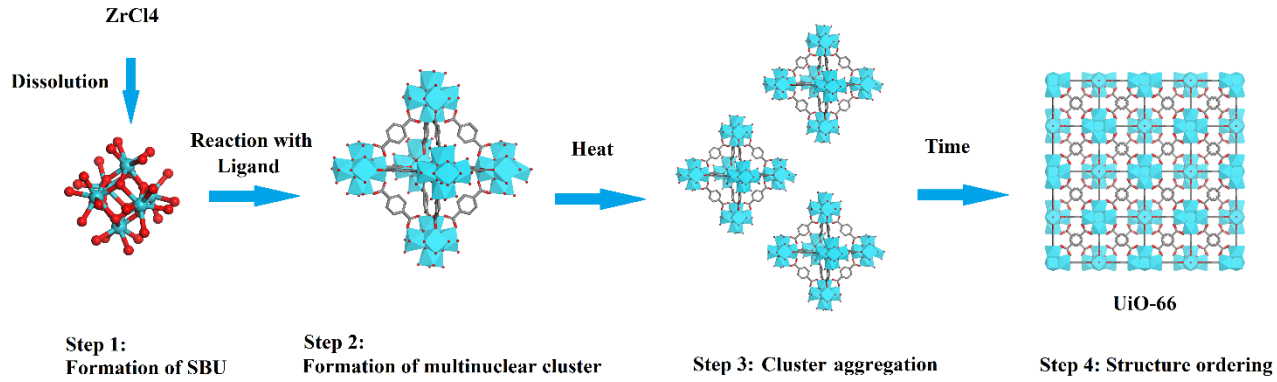

Figure 6. The structure of the species detected by PDF during nucleation and early growth of UiO-66 nanoparticle

Conclusion

In conclusion, the present *in situ* PDF study provides one of the first atomic scale view of MOF nucleation and growth, but many details remain to be understood. It is still unclear how the hexanuclear Zr(IV) SBU structure is formed upon hydrolysis of $ZrCl_4$ precursor solution, and what the pathway is for the precursor clusters to become the nanocrystal nucleus. It is also unclear whether the crystal growth is by attachment of monomer units (e.g. the SBUs) or if the larger clusters of several SBUs connected by the organic linker coalesce. It remains to be seen whether the formation observed for UiO-66 is general for MOF systems and indeed it is of considerable interest to perform similar studies for other MOF systems. If a general structural view of MOF synthesis can be obtained, it allows for optimization of existing experimental protocols and may be suggestive for development of new MOFs.

Experimental Section

Zr(IV) in DMF-HCl solution: $ZrCl_4$ (0.45 g, 1.93 mmol) (Sigma Aldrich, ≥99.9%) was dissolved in N,N'- dimethylformamide (DMF) (8.3 mL, 13.7 mmol) (Sigma Aldrich, ≥99%) and HCl (1.66 mL) (Sigma Aldrich, 37 wt. % in H_2O) at room temperature, and magnetically stirred for an hour to obtain a transparent solution (pH = 1.8). Descriptions of the preparations of the other Zr(IV) solutions are provided in supporting information.

UiO-66 precursor solution: The synthesis procedure is based upon the study of Cavka and Lillerud,[19] with changes suggested by Serre *et al*.[9c] and Gascon *et al*.[10b] A high concentration of the precursor is used in order to obtain high PDF signal, and a high heating temperature was used in order to speed up the reaction. 10 mL Zr(IV) in DMF-HCl solution was prepared the same way as the above. Then 2-Aminoterephthalic Acid (2-NH_2-BDC, 0.33 g, 1.82 mmol) (Sigma Aldrich, 99%) was added into the solution, and magnetically stirred for about an hour to obtain a transparent yellow solution (pH = 1.8).

Total X-ray scattering measurements: The *ex situ* total scattering measurements of different Zr(IV) solutions were carried out at beamline ID-31 at ESRF, Grenoble. The solutions were loaded in kapton capillaries (diameter = 1 mm). The *in situ* total scattering PDF experiments were performed at beam-line P02.1 at PETRAIII, DESY, Germany. The *in situ* total scattering measurement of UiO-66 synthesis was carried out by loading the UiO-66 precursor solution into a fused silica capillary reactor pressurized to 103 bar and heated to temperature 150 ℃. The experimental setup used for *in situ* total scattering has been described by Becker *et al*.[29]

Data treatment: The raw two-dimensional data was integrated with the program Dioptas[30] to obtain total scattering data. Then the total scattering structure factor S(Q) were Fourier transformed using the xPDFsuite software.[31] Prior to the Fourier transformation, the data were corrected for background scattering using measurements corresponding to pure solvents at identical conditions. The resulting PDF for different Zr(IV) solutions and UiO-66 precursor solution were refined using the Diffpy-CMI software based on the Debye function.[20] The UiO-66 synthesis *in situ* PDFs were refined sequentially using the PDFgui software, which is based on the crystallographic approach. The structural refinement of the aqueous Zr(IV) solution is based on crystallographic data of tetragonal $[Zr_4(OH)_8(OH_2)_{16}]^{8+}$ from ICSD-27437.[22c] The structural refinement of UiO-66 precursor and UiO-66 is based on crystallographic data from ICSD-4512072.[19] The PXRD data were refined using Rietveld method in the *FullProf* Suite.[32]

Acknowledgements

Steinar Birgisson, Lirong Song, Dipankar Saha, Aref Hasen Mamakhel, Ann-Christine Dippel, Hazel Readon, Yin Hao and

Mirijam Zobel are thanked for fruitful discussions and assistance with the synthesis, measurements and analysis. This work is supported by the Danish National Research Foundation (DNRF93). H. X. acknowledge financial support from the National Natural Science Foundation of China (51602301). The ESRF and PETRAIII synchrotron facilities are sincerely thanked for beam time. Affiliation with the Aarhus University Center for Integrated Materials Research (iMAT) is gratefully acknowledged.

Notes and references

Throughout the article, the term “crystallite” will be used to describe atoms which assemble into long range structures, while “particles” is used to describe both the crystalline as well as the amorphous structure of an assembly of atoms. “Clusters” is used to describe small, non-random units of atoms, such as the ones displayed in Figure 1. The terms “precursor cluster” or “prenucleation cluster” are used to describe the clusters formed in a precursor solution at room temperature. In this article the presumed MOF multi-SBUs should be understood as a prenucleation cluster.

[1] a)S. Kitagawa, *Chem. Soc. Rev.* **2014**, *43*, 5415-5418; b)H. Kim, Y. Yang, S. R. Rao, S. Narayanan, E. A. Kapustin, H. Furukawa, A. S. Umans, O. M. Yaghi, E. N. Wang, *Science* **2017**, *356*, 430-434; c) Furukawa, K. E. Cordova, M. O'Keeffe, O. M. Yaghi, *Science* **2013**, *341*, 1230444; d)A. Cadiau, K. Adil, P. Bhatt, Y. Belmabkhout, M. Eddaoudi, *Science* **2016**, *353*, 137-140.

[2] a)S. Yuan, L. Feng, K. Wang, J. Pang, M. Bosch, C. Lollar, Y. Sun, J. Qin, X. Yang, P. Zhang, *Adv. Mater.* **2018**; b)C. S. Diercks, Y. Liu, K. E. Cordova, O. M. Yaghi, *Nat. Mater.* **2018**, 1; c)M. O'Keeffe, M. A. Peskov, S. J. Ramsden, O. M. Yaghi, *Acc. Chem. Res.* **2008**, *41*, 1782-1789.

[3] a)N. D. Loh, S. Sen, M. Bosman, S. F. Tan, J. Zhong, C. A. Nijhuis, P. Král, P. Matsudaira, U. Mirsaidov, *Nat. Chem.* **2016**; b)J. J. De Yoreo, N. A. Sommerdijk, *Nature Reviews Materials* **2016**, *1*, 16035.

[4] H. Mistry, A. S. Varela, S. Kühl, P. Strasser, B. R. Cuenya, *Nature Reviews Materials* **2016**, *1*, 16009.

[5] J. H. Seinfeld, S. N. Pandis, *Atmospheric chemistry and physics: from air pollution to climate change*, John Wiley & Sons, **2016**.

[6] a)G. M. Pound, V. K. L. Mer, *J. Am. Chem. Soc.* **1952**, *74*, 2323-2332; b)M. Avrami, *The Journal of Chemical Physics* **1939**, *7*, 1103-1112; c)J. De Yoreo, *Nat. Mater.* **2013**, *12*, 284-285.

[7] R. I. Walton, F. Millange, *The Chemistry of Metal? Organic Frameworks: Synthesis, Characterization, and Applications? Synthesis, Characterization, and Applications* **2016**, 729-764.

[8] a)J. Zhao, B. Kalanyan, H. F. Barton, B. A. Sperling, G. N. Parsons, *Chem. Mater.* **2017**, *29*, 8804-8810; b)D. Zacher, R. Schmid, C. Wöll, R. A. Fischer, *Angew. Chem. Int. Ed.* **2011**, *50*, 176-199; c)R. Wang, I. Strashnov, M. W. Anderson, M. P. Attfield, *Angew. Chem. Int. Ed.* **2016**, *55*, 9075-9079; d)J. P. Patterson, P. Abellan, M. S. Denny, C. Park, N. D. Browning, S. M. Cohen, J. E. Evans, N. C. Gianneschi, *J. Am. Chem. Soc.* **2015**, *137*, 7322-7328; e)J. Cravillon, R. Nayuk, S. Springer, A. Feldhoff, K. Huber, M. Wiebcke, *Chem. Mater.* **2011**, *23*, 2130-2141; f)D. Biswal, P. G. Kusalik, *ACS nano* **2016**, *11*, 2589-268; g)T. Birsa Čelič, M. Rangus, K. Lázár, V. Kaučič, N. Zabukovec Logar, *Angew. Chem. Int. Ed.* **2012**, *51*, 12490-12494; h)R. Ameloot, F. Vermoortele, J. Hofkens, F. C. De Schryver, D. E. De Vos, M. B. Roeffaers, *Angew. Chem. Int. Ed.* **2013**, *52*, 401-405.

[9] a)H. H. M. Yeung, Y. Wu, S. Henke, A. K. Cheetham, D. O'Hare, R. I. Walton, *Angew. Chem.* **2016**, *128*, 2052-2056; b)Y. Wu, M. Breeze, G. J. Clarkson, F. Millange, D. O'Hare, R. I. Walton, *Angew. Chem. Int. Ed.* **2016**, *55*, 4992-4996; c)F. Ragon, P. Horcajada, H. Chevreau, Y. K. Hwang, U.-H. Lee, S. R. Miller, T. Devic, J.-S. Chang, C. Serre, *Inorg. Chem.* **2014**, *53*, 2491-2500; d)F. Millange, M. I. Medina, N. Guillou, G. Férey, K. M. Golden, R. I. Walton, *Angew. Chem. Int. Ed.* **2010**, *49*, 763-766; e)P. A. Julien, K. Užarević, A. D. Katsenis, S. A. Kimber, T. Wang, O. K. Farha, Y. Zhang, J. Casaban, L. S. Germann, M. Etter, *J. Am. Chem. Soc.* **2016**, *138*, 2929-2932.

[10] a)E. Stavitski, M. Goesten, J. Juan - Alcañiz, A. Martinez - Joaristi, P. Serra - Crespo, A. V. Petukhov, J. Gascon, F. Kapteijn, *Angew. Chem. Int. Ed.* **2011**, *50*, 9624-9628; b)M. Goesten, M. De Lange, A. Olivos-Suarez, A. Bavykina, P. Serra-Crespo, C. Krywka, F. Bickelhaupt, F. Kapteijn, J. Gascon, *Nat. Commun.* **2016**, *7*; c)J. Cravillon, C. A. Schröder, R. Nayuk, J. Gummel, K. Huber, M. Wiebcke, *Angew. Chem.* **2011**, *123*, 8217-8221.

[11] A. Schoedel, O. M. Yaghi, *The Chemistry of Metal? Organic Frameworks: Synthesis, Characterization, and Applications: Synthesis, Characterization, and Applications*, 41-72.

[12] a)A. Schoedel, M. J. Zaworotko, *Chem. Sci.* **2014**, *5*, 1269-1282; b)M. Bosch, S. Yuan, W. Rutledge, H.-C. Zhou, *Acc. Chem. Res.* **2017**, *50*, 857-865.

[13] a)S. Surble, F. Millange, C. Serre, G. Ferey, R. I. Walton, *Chem. Commun.* **2006**, 1518-1520; b)M. Haouas, C. Volkringer, T. Loiseau, G. r. Férey, F. Taulelle, *Chem. Mater.* **2012**, *24*, 2462-2471; c)G. r. Férey, M. Haouas, T. Loiseau, F. Taulelle, *Chem. Mater.* **2014**, *26*, 299-309.

[14] M. Shoaee, M. W. Anderson, M. P. Attfield, *Angew. Chem.* **2008**, *120*, 8653-8656.

[15] T. Egami, S. J. Billinge, *Underneath the Bragg peaks: structural analysis of complex materials, Vol. 16*, Elsevier, **2003**.

[16] a)M. Zobel, R. B. Neder, S. A. Kimber, *Science* **2015**, *347*, 292-294; b)D. Saha, K. M. Jensen, C. Tyrsted, E. D. Bøjesen, A. H. Mamakhel, A. C. Dippel, M. Christensen, B. B. Iversen, *Angew. Chem. Int. Ed.* **2014**, *53*, 3667-3670; c)P. Nørby, S. Johnsen, B. B. Iversen, *ACS nano* **2014**, *8*, 4295-4303; d)K. M. Jensen, M. Christensen, P. Juhas, C. Tyrsted, E. D. Bøjesen, N. Lock, S. J. Billinge, B. B. Iversen, *J. Am. Chem. Soc.* **2012**, *134*, 6785-6792; e)E. D. Bøjesen, K. M. Jensen, C. Tyrsted, A. Mamakhel, H. L. Andersen, H. Reardon, J. Chevalier, A.-C. Dippel, B. B. Iversen, *Chem. Sci.* **2016**, *7*, 6394-6406.

[17] A. E. Platero-Prats, A. Mavrandonakis, L. C. Gallington, Y. Liu, J. T. Hupp, O. K. Farha, C. J. Cramer, K. W. Chapman, *J. Am. Chem. Soc* **2016**, *138*, 4178-4185.

[18] M. W. Terban, D. Banerjee, S. Ghose, B. Medasani, A. Shukla, B. A. Legg, Y. Zhou, Z. Zhu, M. L. Sushko, J. J. De Yoreo, *Nanoscale* **2018**, *10*, 4291-4300.

[19] J. H. Cavka, S. Jakobsen, U. Olsbye, N. Guillou, C. Lamberti, S. Bordiga, K. P. Lillerud, *J. Am. Chem. Soc.* **2008**, *130*, 13850-13851.

[20] P. Juhás, S. Billinge, *Foundations of Crystallography* **2017**, *73*, a388.

[21] T. D. Bennett, T. K. Todorova, E. F. Baxter, D. G. Reid, C. Gervais, B. Bueken, B. Van de Voorde, D. De Vos, D. A. Keen, C. Mellot-Draznieks, *Physical Chemistry Chemical Physics* **2016**, *18*, 2192-2201.

[22] a)C. Walther, J. Rothe, M. Fuss, S. Büchner, S. Koltsov, T. Bergmann, *Anal Bioanal Chem* **2007**, *388*, 409-431; b)N. Rao, M. N. Holerca, V. Pophristic, *J Chem Theory Comput* **2008**, *4*, 145-155; c)C. Hennig, S. Weiss, W. Kraus, J. Kretzschmar, A. C. Scheinost, *Inorg. Chem.* **2017**, *56*, 2473-2480; d)A.-C. Dippel, K. Jensen, C. Tyrsted, M. Bremholm, E. D. Bøjesen, D. Saha, S. Birgisson, M. Christensen, S. J. Billinge, B. B. Iversen, *Acta Crystallographica Section A: Foundations and Advances* **2016**, *72*, 645-650.

[23] A. Clearfield, P. A. Vaughan, *Acta Crystallographica* **1956**, *9*, 555-558.

[24] C. Tyrsted, N. Lock, K. Jensen, M. Christensen, E. D. Bøjesen, H. Emerich, G. Vaughan, S. J. Billinge, B. B. Iversen, *IUCrJ* **2014**, *1*, 165-171.

[25] a)T. D. Bennett, A. K. Cheetham, *Acc. Chem. Res.* **2014**, *47*, 1555-1562; b)G. C. Shearer, S. Chavan, S. Bordiga, S. Svelle, U. Olsbye, K. P. Lillerud, *Chem. Mater.* **2016**, *28*, 3749-3761.

[26] a)G. r. Férey, M. Haouas, T. Loiseau, F. Taulelle, *Chem. Mater.* **2013**, *26*, 299-309; b)I. H. Lim, W. Schrader, F. Schüth, *Chem. Mater.* **2015**, *27*, 3088-3095.

[27] C. Granados-Miralles, M. Saura-Múzquiz, E. D. Bøjesen, K. M. Jensen, H. L. Andersen, M. Christensen, *J. Mater. Chem. C* **2016**, *4*, 10903-10913.

[28] a)D. Gebauer, M. Kellermeier, J. D. Gale, L. Bergström, H. Cölfen, *Chem. Soc. Rev.* **2014**, *43*, 2348-2371; b)E. D. Bøjesen, B. B. Iversen, *Crystengcomm* **2016**, *18*, 8332-8353.

[29] J. Becker, M. Bremholm, C. Tyrsted, B. Pauw, K. Jensen, J. Eltzholt, M. Christensen, B. B. Iversen, *J. Appl. Crystallogr.* **2010**, *43*, 729-736.

[30] C. Prescher, V. B. Prakapenka, *High Pressure Research* **2015**, *35*, 223-230.

[31] P. Juhás, T. Davis, C. L. Farrow, S. J. Billinge, *J. Appl. Crystallogr.* **2013**, *46*, 560-566.

[32] J. Rodríguez-Carvajal, *Physica B: Condensed Matter* **1993**, *192*, 55-69.

Entry for the Table of Contents

COMMUNICATION

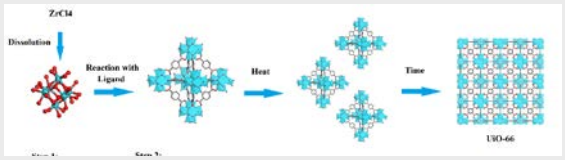

*Hui Xu, Sanna Sommer, Nils Lau Nyborg Broge, Junkuo Gao and Bo. B. Iversen**

Page No. – Page No.

The Chemistry of Nucleation: in situ Pair Distribution Function analysis of secondary building units during UiO-66 MOF formation

In situ PDF analysis was used to reveal the atomic scale nature of precursor species during solvothermal UiO-66 MOF synthesis, and a hexanuclear zirconium cluster was established as the secondary building unit present even in the metal salt precursor solution.